Proceedings of ASME Turbo Expo 2019
Turbo Expo 2019
June 17-21, 2019, Phoenix AZ, USA

GT2019-91473

STUDY OF DYNAMICAL INSTABILITIES IN SIEMENS LIQUID SPRAY INJECTORS USING COMPLEMENTARY MODAL DECOMPOSITION TECHNIQUES

Adesile Ajisafe[1], Midhat Talibi[*1], Andrea Ducci[1], Ramanarayanan Balachandran[1], Nishant Parsania[2], Suresh Sadusivuni[2], Ghenadie Bulat[2]
[1]Department of Mechanical Engineering, University College London, London WC1E 7JE, UK
[2]Siemens Industrial Turbomachinery Ltd., Ruston House, Waterside South, Lincoln LN5 7FD, UK.

ABSTRACT

Liquid fuel spray characterisation is essential for understanding the mechanisms underlying fuel energy release and pollutant formation. Careful selection of operating conditions can promote flow instabilities in the fuel spray which can enhance atomisation and fuel mixing, thereby resulting in more efficient combustion. However, the inherent instabilities present in the spray could have adverse effect on the combustor dynamics. Hence, it is important to better understand the dynamical behaviour of the spray, and particularly at representative operating conditions. This work describes an experimental investigation of dynamical behaviour of pressure-swirl atomisers used in Siemens industrial gas turbine combustors, at a range of chamber pressures and fuel injection pressures, using high speed laser planar imaging. Two modal decomposition techniques - Proper Orthogonal Decomposition (POD) and Dynamic Mode Decomposition (DMD) - are applied and compared to assess the spray dynamics. Results indicate that both POD and DMD are able to capture periodic structures occurring in the spray at different spatial length scales. The characteristic frequencies estimated from both the methods are in good agreement with each other. Both techniques are able to identify coherent structures with variable size, shape and level of staggering, which are observed to be dependent on the pressure difference across the atomiser and the chamber pressure. The spatio-temporally resolved data and the results could be used for spray model development and validation. Furthermore, the methods employed could be applied to other fuel atomisers, and more complicated conditions involving cross flow and higher chamber temperatures.

NOMENCLATURE

DLE	Dry Low Emissions
DMD	Dynamic Mode Decomposition
MDT	Modal Decomposition Technique
ROM	Reduced Order Model
POD	Proper Orthogonal Decomposition
PSD	Power Spectral Density
Δp	Pressure difference across the fuel injector
λ	POD eigenvalue
σ	Growth/decay rate of a DMD mode
ω	Angular frequency of a DMD mode
Φ	Spatial mode of either POD or DMD
μ	DMD eigenvalue
$a_n(t)$	Temporal coefficient of POD modes
I	Greyscale Intensity field
f	Frequency
N	Number of snapshots/images
p_F	Fuel pressure
p_A	Ambient/chamber pressure
r	DMD Residual
Re	Reynolds number

[*]Corresponding author. m.talibi@ucl.ac.uk

1 INTRODUCTION

Lean burn technology is commonly employed to achieve ultra-low NOx emissions in gas turbine engines. Modern low emission gas turbine engines often utilise pressure swirl atomisers for direct injection of fuel into the air-stream either in co- or cross- flow configurations for lean burn operation. The swirl and high pressures inside the atomisers enable fine atomisation, while cross-flow and/or swirling motion (in co-flow) of air enable rapid mixing. The quality of spray has a direct impact on emissions and combustion performance. The common industrial design approach is to identify spray geometric parameters (statistical quantities, such as spray cone angle and penetration length) from experiments and/or modelling and relate them to the quality of the spray. However, this approach is rather crude and does not contemplate and exploit any knowledge of the inherent dynamical characteristics of sprays. The dynamical characteristics observed during spray formation and its interaction with air are associated with various instability mechanisms such Rayleigh-Taylor, Kelvin-Helmholtz, etc. [1–4]. In lean burn combustion systems, the spray dynamics could contribute to self-excited combustion oscillations [5]. Hence, it is important to understand the dynamical behaviour of sprays and develop appropriate correlations to best describe spray quality.

Modal decomposition techniques, MDTs, are often employed in fluid mechanics to identify large scale coherent structures, which are responsible for mass and kinetic energy transfer and/or are related to flow instabilities. Among the different modal decomposition techniques available in the literature Proper Orthogonal Decomposition, POD, and Dynamic Mode Decomposition, DMD, are those which have been most widely used in a broad range of engineering applications, including chemical and biochemical processes [6, 7], combustion [8, 9], aerodynamics [10] to mention a few. POD ranks modes in terms of kinetic energy content, while its temporal modes might be associated to more than one frequency. On the contrary, each mode in DMD is associated to a single angular frequency, ω, and rate of growth/decay, σ, and it is therefore more efficient at capturing the dynamical behaviour of a system.

The main feature of all MDTs is decoupling the spatial and temporal length scales of a flow into a series of pairs of temporal and spatial functions, with each pair related to a specific mode. Analysis of the temporal function allows to isolate specific frequencies, either related to natural (i.e. vortex shedding frequency in cylinder flows, [11]) or forced (i.e. blade passage frequency in a stirred tank, [12, 13]) flow oscillations, and link them to spatial structures, thus providing a thorough description of a specific coherent structure. In this perspective, selection of the most dominant structures (i.e. modes) based on their energy content can lead to the formulation of Reduced Order Models, ROMs, where the selected modes are linearly superimposed, while least energetic modes related to finer scales, turbulence and/or noise, are filtered out. When considering the implementation of a flow control system in a real-time application, ROMs offer a simplified description of its dynamical behaviour, and can be used and adapted towards the development of efficient control strategies [14, 15].

In combustion and spray dynamics an extended dynamic mode decomposition methodology has been simultaneously applied to the flame and velocity fields obtained by Large Eddy Simulation, LES, in a lean premixed low swirl stabilised methane/air flame at Re=20000 [9]. This analysis allowed the characterisation of complex flow-flame interactions in the burner, and identification of low frequency spatial structures, at 175 hz and 211 hz, which were found to dominate the inner and outer shear layers of the flow, respectively. Similarly Bourgouin *et al.* employed DMD to assess to what extent the mean and unsteady flow structures were affected by small variations of a swirler design in a combustor [8]. It was found that small variations of the swirler geometry nearly doubled the frequency (765 hz to 1378 hz) of the precessing vortex core, PVC, dominating the flow downstream of the nozzle for Re=7600 (based on injection tube diameter). Similarly, POD has been extensively applied to various combustion problems, such as combustion dynamics, lean blowout, etc. [16–18].

Advancements in measurement methods, computing technologies and improvements in modal analysis approaches have enabled effective application of these techniques to various practical problems. However, the use of such techniques to characterise sprays from industrial fuel atomisers at practical operating conditions are challenging. In this work, POD and DMD techniques are applied to understand the dynamical behaviours of an industrial fuel atomiser. The specific objectives of this work are i) to identify dominant dynamical features by applying POD/DMD methods on spray images obtained using laser planar imaging technique (Mie scattering), ii) to evaluate and comment on the effectiveness and complementarity of the two techniques POD/DMD, and iii) understand the effect of variation in key operating parameters of fuel injectors on the dynamical behaviour. The following sections of the paper will provide the context and details of the hardware used, followed by discussion of results related to the two modal analysis techniques and summary of key findings.

2 SIEMENS SGT DLE COMBUSTION SYSTEM

Siemens Industrial Turbomachinery Ltd in Lincoln, UK is the manufacturer of small industrial gas turbines from the SGT-100 at 5 MW to the SGT-400 at 15 MW, and which has now accumulated more than 40 million hours of operational experience on DLE (Dry Low Emissions) systems. The dual fuel DLE combustion system is designed as a reverse-flow can-annular type, as shown in Fig. 1.

The combustor consists of three main sections: (1) the pilot burner, which houses the pilot fuel galleries and injectors for

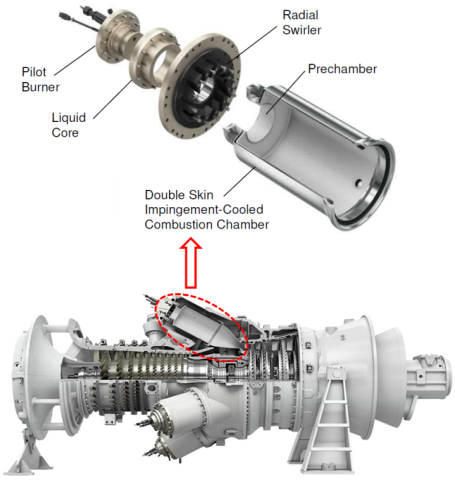

FIGURE 1. SIEMENS DLE COMBUSTOR CONFIGURATION.

both gaseous and liquid fuel; (2) the main burner, which houses the main air swirler and main gas and liquid fuel system; (3) the combustor, which includes the pre-chamber, has a double skin construction and is cooled through impingement cooling. Downstream of the combustor, a transition duct is used to condition the flow from the circular combustor exit to a sector of the turbine entry annulus. In order to cover the full range of power, rather than having a single combustor design and applying different numbers of combustor to each engine type, the combustors have been scaled. The SGT-100, 300 and 400 have 6 combustors per engine and the SGT-200 has 8 cans.

A schematic of the combustion concept is shown in Fig. 2. The main combustion air enters through a single radial swirler at the head of the combustor. The flow then turns through a right angle into the pre-chamber followed by a sudden expansion into the combustion chamber. The swirl number is sufficiently high to induce a vortex breakdown reverse flow zone along the axis. This is termed the internal reverse flow zone. In the concept, this reverse flow zone remains attached to the back surface of the combustor, thereby establishing a firm aerodynamic base for flame stabilisation. In the wake of the sudden expansion, an external reverse flow zone is established. The gas flame is stabilised in the shear layers around the internal and external reverse flow zones [19].

Liquid is injected at two main locations. Main liquid core (as shown in Figs. 1 and 2) and pilot lance (Fig. 2) which is built inside the pilot burner at a specified radial location. This location of the lance is designed in such a way that spray is injected optimally into the primary combustion region reducing emissions and increasing start-up reliability. The liquid core consists of 6 nozzles which are pressure swirl atomisers located in alternative radial slots of the swirler. Liquid lance is also a pressure swirl

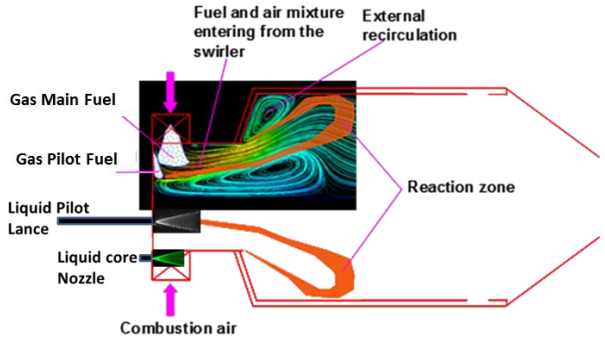

FIGURE 2. SIEMENS DLE COMBUSTION CONCEPT.

atomiser with air assist. Experiments conducted at UCL were performed without any air assist. Liquid cores are subjected to strong cross flow of air which improves the atomisation process. UCL experiments were performed on stationary flow rig with high pressure conditions.

Both gas and liquid fuels are introduced in two stages: the main, which results in a high degree of premixedness and hence low NOx emissions, and the pilot, which is steadily increased as the load demand decreases in order to ensure flame stability. The pilot is arranged, such that as the pilot fuel split increases, the fuel is biased towards the axis of the combustor.

3 METHODOLOGY

3.1 Laser Planar Spray Imaging Setup

The spray measurements were carried out in a high-pressure spray facility, capable of withstanding 100 bar and 800 K, and with four-way orthogonal optical access. The vessel is cylindrical in shape with an inner diameter of 300 mm and internal volume of about 23 litres. Quartz windows are used on the vessel for optical access, with the window bosses allowing a viewing window of 120 mm diameter. Compressed air of high purity (zero grade) was used to increase the vessel pressure (ambient pressure). Diesel surrogate fuel, VISCOR calibration fluid, was pressurised using zero grade compressed nitrogen, and injected into the vessel using Siemens simplex pressure swirl atomisers. In between each test condition, the vessel was exhausted using vacuum pumps in order to reset the environment inside the vessel before proceeding to the next test condition. The gas and fuel supply lines, as well as the vessel are fitted with fast response digital pressure transducers, which provide live readings to the PC via National Instruments (NI) data acquisition systems. In addition, bespoke programs were written in NI LABVIEW software for precise control of the vessel filling and emptying procedures, as well as to synchronise the fuel injection time with the optical diagnostic measurements.

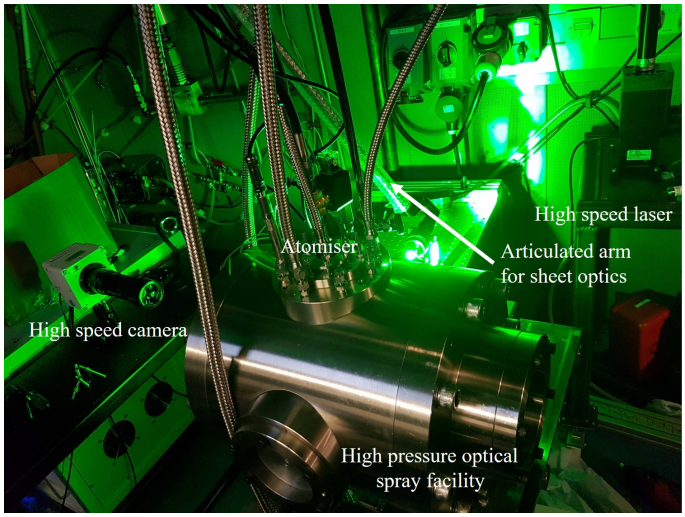

(a)

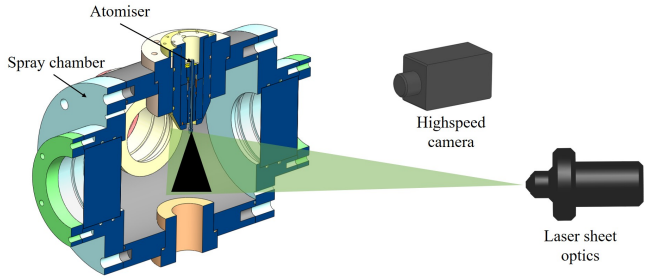

(b)

FIGURE 3. (a) SPRAY TEST FACILITY; (b) SCHEMATIC OF THE EXPERIMENTAL SETUP.

The spray dynamics are captured with laser planar imaging technique (based on Mie scattering) on a vertical plane bisecting the atomiser cross-section (as seen in Fig. 3). High speed imaging of the spray was carried out using a Nd:YLF high speed laser (Litron LDY304-PIV) and a high speed CMOS camera (Phantom VEO710). The camera was fitted with a Nikon (Micro-Nikkor 200 mm) lens. The images were captured at a frame rate of 6700 hz, up to a distance of 20 atomiser tip diameters downstream of the atomiser. Each fuel injection lasted approximately 250 ms, with ≈1500 images captured during the steady state of the spray. TSI Insight 4G software was utilised to capture the images, while in-house developed MATLAB routines were used to post process the data with modal decomposition techniques (see Section 3.2). Two sets of experiments were carried out to assess how flow instabilities were affected by a) varying the pressure difference across the nozzle for a fixed ambient pressure, and b) varying the ambient pressure for a fixed pressure difference across the nozzle. Each set comprised of three test cases where one of the parameters, either the pressure difference, Δp, or the chamber ambient pressure was kept constant. This was achieved

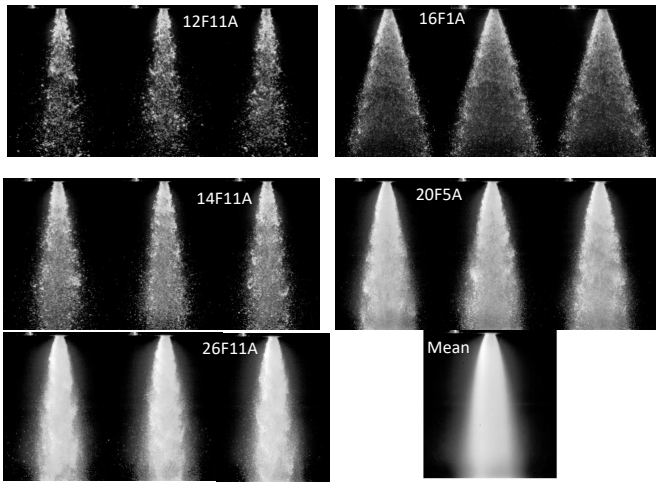

FIGURE 4. THREE INSTANTANEOUS RAW SNAPSHOTS FOR EACH TEST CONDITION AND THE AVERAGED IMAGE OF THE REFERENCE TEST CASE, 26F11A.

by varying the fuel injection pressure, p_F, and chamber (ambient) pressure, p_A. One of the test cases was common between the two sets.

Table 1 lists the specific pressures used for each test case together with the corresponding Reynolds number (estimated by atomiser flow performance data provided by Siemens). In the remainder of the paper, the test cases investigated are denoted as XXFYYA, where XX and YY correspond to the pressure at the fuel and ambient sides of the atomiser, respectively. Typical instantaneous snapshots are given in Fig. 4 (a) for each test case investigated. The presence of coherent structures is evident at the interface between the fuel jet and the ambient air.

TABLE 1. TEST MATRIX.

Test case	p_F [bar]	p_A [bar]	Δp [bar]	Re
12F11A	12	11	1	3400
14F11A	14	11	3	5800
26F11A	26	11	15	13000
16F1A	16	1	15	13000
20F5A	20	5	15	13000

3.2 POD and DMD Techniques

The images captured using laser planar imaging in this study were post-processed with two decomposition techniques,

namely, Proper Orthogonal Decomposition, POD, and Dynamic Mode Decomposition, DMD. The principles and algorithm description employed in Ref. [7] have been adapted for this work. For consistency, the details of the two techniques have been presented here. Both techniques are applied to the snapshot matrix, X, which is obtained by re-arranging the instantaneous intensity fields, $I(\mathbf{x},t)$, along different columns, as shown in Eqn. (1):

$$X = \begin{bmatrix} I(x_1,t_1) & I(x_1,t_2) & ..... & I(x_1,t_N) \\ I(x_2,t_1) & I(x_2,t_2) & ..... & I(x_2,t_N) \\ \vdots & \vdots & \vdots & \vdots \\ \vdots & \vdots & \vdots & \vdots \\ I(x_M,t_1) & I(x_M,t_2) & ..... & I(x_M,t_N) \end{bmatrix} \quad (1)$$

The size of X is $M \times N$, where M and N are the number of locations within the image intensity field and the number of time instants collected, respectively. POD is a linear technique, based on temporal and spatial correlation analysis, that decomposes a set of signals into a modal base with modes ordered in terms of "energy" content (i.e. decreasing eigenvalues, λ, of the correlation tensor, $X^T \cdot X$ see [6]). The first few modes are the most energetic and associated with large scale structures, whereas the last modes are the least energetic and related to the small scale structures and turbulence. In Eqn. (2), the POD analysis is applied to the fluctuating part of the intensity distribution, $I'(\mathbf{x},t)$:

$$I(\mathbf{x},t) = \bar{I}(\mathbf{x}) + I'(\mathbf{x},t) = \bar{I}(\mathbf{x}) + \sum_{n=1}^{N_s} a_n(t)\Phi_n(\mathbf{x}) \quad (2)$$

where $I(\mathbf{x},t)$ and $\bar{I}(\mathbf{x})$ are the instantaneous and mean intensity fields, respectively, whereas, Φ_n and a_n are the spatial eigenfunction and the temporal coefficient associated to the n^{th} mode, respectively. Depending on the system investigated a Reduced Order Model, ROM, can be utilised to reconstruct the large scale flow features and filter out turbulence and experimental error. The ROM would comprise of a small number of modes that are characterised by large "energy" content. A detailed description of POD can be found in [20].

An alternative decomposition technique is DMD, which was first proposed by Schmid [21], and allows a better insight into the dynamics of a system. DMD assumes a linear correlation between consecutive snapshots, as indicated in Eqn. (3):

$$I_{i+1} = A\, I_i \quad (3)$$

where I_{i+1} and I_i are two adjacent columns of X. This linear correlation can be formulated for all the columns of X according to Eqn. (4):

$$X_N = A\, X_{N-1} \quad (4)$$

where X_{N-1} and X_N are sub-matrices of X including the first and last $N-1$ columns, respectively. When the number of snapshots included in X is large enough, it is possible to assume that its last column, I_N, becomes linearly dependent of the previous ones, and a base of $N-1$ snapshots is sufficient to reconstruct I_N according to Eqn. (5):

$$I_N = c_1 I_1 + c_2 I_2 + ... + c_{N-1} I_{N-1} + r \quad (5)$$

where r is a residual and c_i are coefficients.

The singular value decomposition of the snapshot submatrix X_{N-1} is computed according to Eqn. (6):

$$X_{N-1} = U \Sigma V^* \quad (6)$$

where matrices U and V contain the spatial structure and the temporal coefficient of the modes, respectively, while Σ provides the energy ranking of the modes. The asterisk in Eqn. (6) denotes a matrix complex conjugate transpose.

The eigenvalues, μ, of A come in complex conjugate pairs and provide information on the temporal stability and dynamic characteristics of the modes. The eigenvalue, μ, are used in Eqns. (7) and (8) to estimate the exponential increase/decay, σ, and angular frequency, ω, of each mode.

$$\sigma = \frac{\log(|\mu|)}{\Delta t} \quad (7)$$

$$\omega = 2\pi f = \frac{\arg(\mu)}{\Delta t} \quad (8)$$

where Δt is the time delay between two consecutive snapshots.

The DMD spatial modes are estimated according to Eqn. (9), where U is projected on y_i, which is the ith eigenvector of the linear coefficient matrix, A.

$$\Phi_i = U y_i \quad (9)$$

A detailed description of the DMD can be found in the works of [21] and [22].

In agreement with the work of [11] a residual analysis was carried out to optimise the number of snapshots N to be included in the matrix X. This is reported in Fig. 5, where three different types of residuals were calculated for increasing size of X.

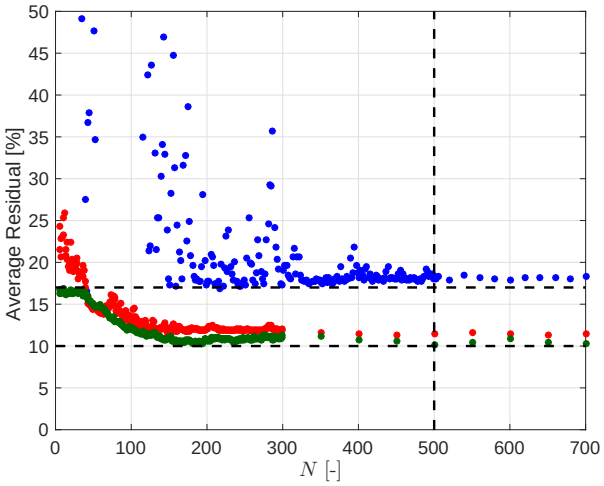

FIGURE 5. AVERAGE RESIDUAL WITH NUMBER OF SNAPSHOTS, N, USED IN DMD: (•)RESIDUAL OF THE N^{th} SNAPSHOT; (•) AVERAGE RESIDUAL OF THE 120 SNAPSHOTS AFTER N; (•) AVERAGE RESIDUAL OF SNAPSHOTS 900-1000.

For all cases DMD was applied to the first N snapshots out of a sample of a 1000 images. The residual reported in green in Fig. 5 corresponds to that obtained from the reconstruction of Eqn. (5) . This is the standard residual usually estimated in any DMD application. The residual in red is an average of the first 120 snapshots after the N^{th} image, while the residual in blue corresponds to the reconstruction of the last 100 snapshots out of the 1000 sample. In all cases it is possible to see that the residuals level off with increasing N. As expected the blue residual is the largest, as in this case there is an attempt to reconstruct/predict events occurring with a significant delay with respect to the N snapshots used in the DMD analysis. From Fig. 5, a size of 500 snapshots was deemed sufficient to best describe the system, as all the residuals did not manifest a significant decay for $N > 500$.

4 RESULTS AND DISCUSSIONS

4.1 POD Analysis

The variation of the eigenvalues, presented as a fraction of the total energy, are shown in Fig. 6 (a) and (b) for varying pressure difference and constant Δp, respectively. The first mode, which is related to the mean flow, contained between 7-28 % of the total energy, depending on the test case investigated, and is not shown in Fig. 6 for clarity of presentation. The first 9 modes after the mean contained 3-5 % of the remaining energy and were investigated in more detail. From Fig. 6 (a) it is evident that a higher value of Δp determines sharper drop of λ over the first 9 modes. This aspect is observed to a lesser extent in Fig. 6 (b) where all test cases were obtained for the same pressure drop and therefore exhibit a similar variation in eigenvalue fraction.

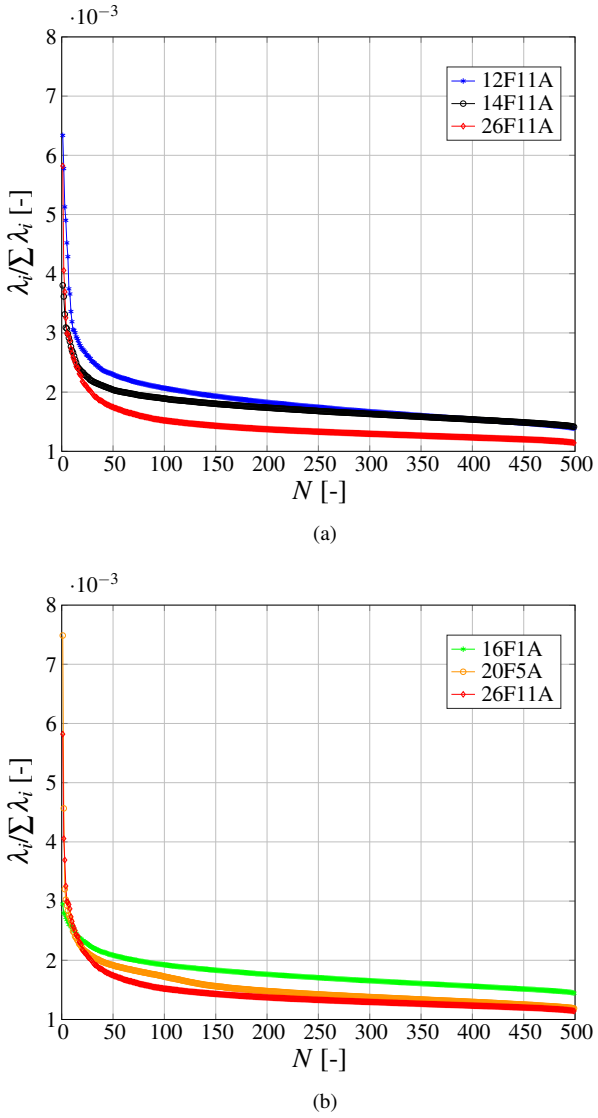

FIGURE 6. VARIATION OF ENERGY FRACTION WITH POD MODE NUMBER, N; (a) CONSTANT AMBIENT PRESSURE; (b) CONSTANT PRESSURE DIFFERENCE, Δp.

A visualisation of the first nine spatial modes, mean mode excluded, is provided in Figs. 7-11 for all the test cases considered (mode 0, which is related to the mean flow, is not shown). Several coherent structures can be seen in each mode, with their size decreasing as higher modes are considered. This behaviour is expected since POD orders modes in terms of their "energy" content, and therefore finer scale structures should occur in higher modes. When comparing test cases for a fixed constant ambient pressure (Figs. 7-9) it is evident that an increase in pressure difference corresponds to coherent structures larger in size, further apart in the axial direction and with a higher degree of staggering. The latter aspect is most pronounced in Fig. 9 for

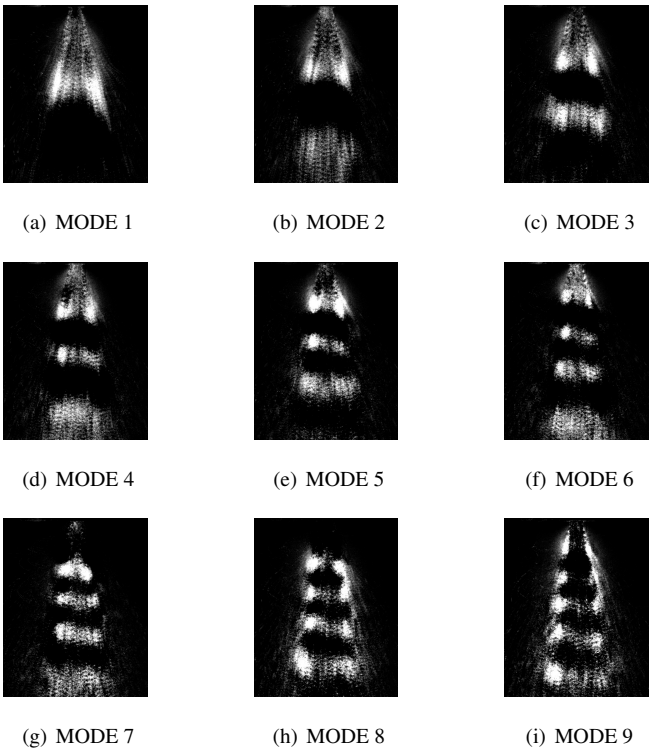

(a) MODE 1 (b) MODE 2 (c) MODE 3

(d) MODE 4 (e) MODE 5 (f) MODE 6

(g) MODE 7 (h) MODE 8 (i) MODE 9

FIGURE 7. POD SPATIAL MODES FOR 12F11A CASE.

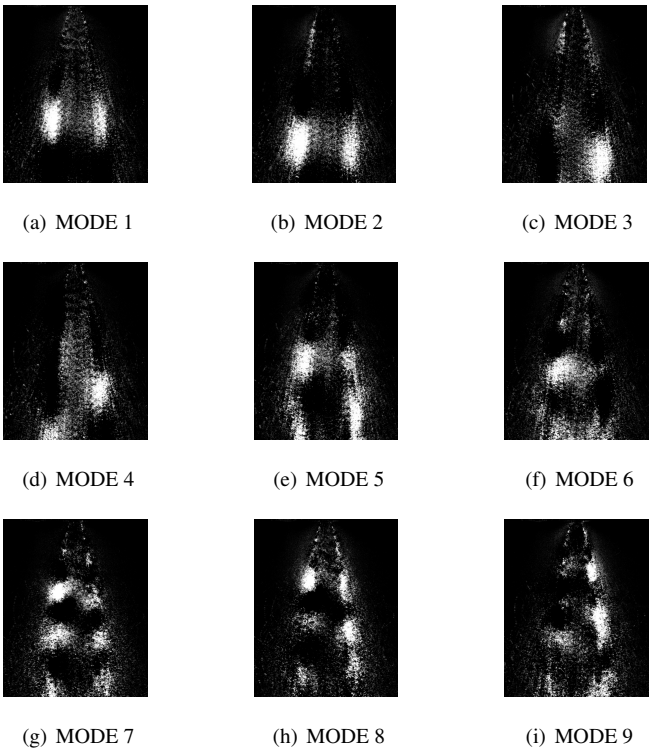

(a) MODE 1 (b) MODE 2 (c) MODE 3

(d) MODE 4 (e) MODE 5 (f) MODE 6

(g) MODE 7 (h) MODE 8 (i) MODE 9

FIGURE 8. POD SPATIAL MODES FOR 14F11A CASE.

$\Delta p = 15$ bar (i.e. 26F11A), which is the highest fuel injection and chamber pressure investigated. These variations can be explained by considering that a higher pressure difference between the liquid jet and the ambient air produces oscillations at the interface of higher amplitude and larger wavelength. The degree of staggering is directly related to the convective velocity and the oscillation growth rate, and could be linked to shear layer instabilities characterised by a helical shape. From this perspective a high Δp, corresponding to a greater convection velocity, would impart a stretching of the helix, which is reflected in the pronounced staggered formation of Fig. 9. This progressive change in the spatial mode shapes with increasing fuel pressure can be beneficial for fine atomisation.

When the chamber pressure is decreased Figs. 9-11, for a fixed Δp=15 bar, equivalent mode numbers exhibit a decreasing number of coherent structures, which are characterised by a reduction in size and in the level of staggering. This effect is more pronounced for the 16F1A (see Fig. 10), where the structures are closer. This might be linked to the fuel-ambient air density ratio: for example, only a two-fold increase in ρ_F/ρ_A occurs between test cases 26F11A and 20F5A, while ten-fold and five-fold increase were observed between the lowest pressure data set investigated (16F1A) and the other two. Though atomisation can be improved by either changing the fuel injection pressure or the ambient pressure, the POD shows that the dynamical behaviour

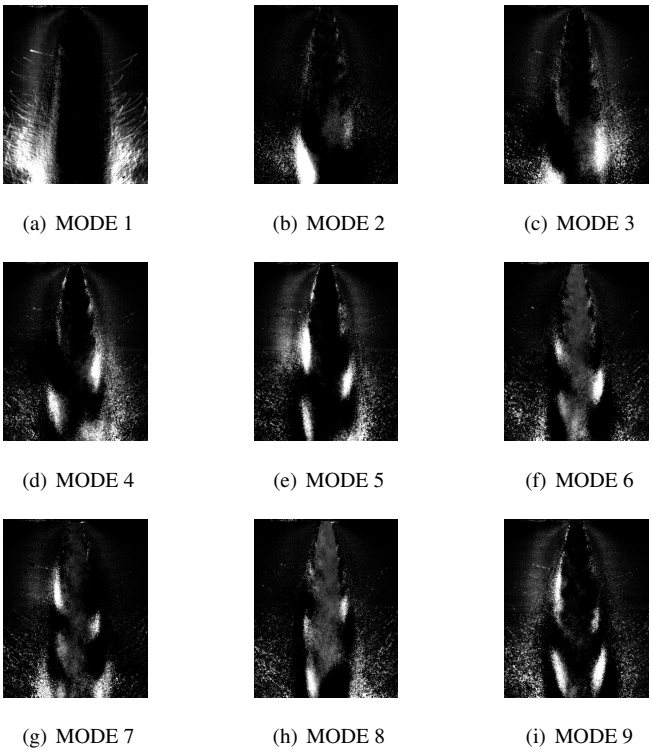

(a) MODE 1 (b) MODE 2 (c) MODE 3

(d) MODE 4 (e) MODE 5 (f) MODE 6

(g) MODE 7 (h) MODE 8 (i) MODE 9

FIGURE 9. POD SPATIAL MODES FOR 26F11A CASE.

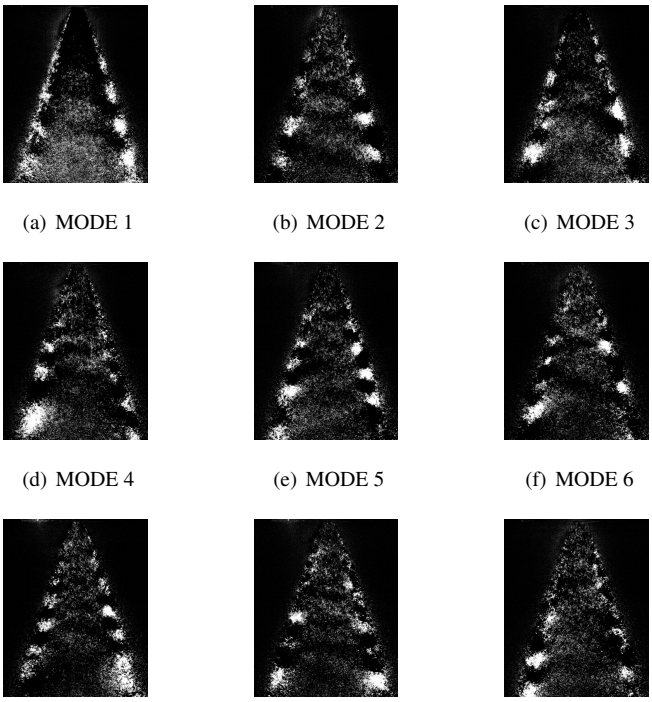

(a) MODE 1 (b) MODE 2 (c) MODE 3

(d) MODE 4 (e) MODE 5 (f) MODE 6

(g) MODE 7 (h) MODE 8 (i) MODE 9

FIGURE 10. POD SPATIAL MODES FOR 16F1A CASE.

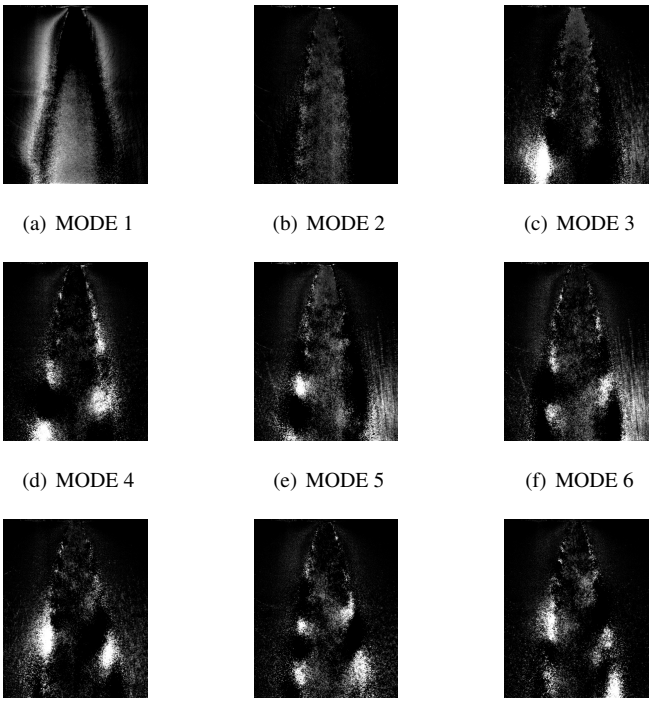

(a) MODE 1 (b) MODE 2 (c) MODE 3

(d) MODE 4 (e) MODE 5 (f) MODE 6

(g) MODE 7 (h) MODE 8 (i) MODE 9

FIGURE 11. POD SPATIAL MODES FOR 20F5A CASE.

of sprays could be different for these two approaches.

Figure 12 shows the power spectrum density (PSD) of the POD temporal coefficients, normalised by their maximum values, of the first nine modes for the reference test case (26F11A). The PSD was calculated using Welch's method [23]. It is evident from this figure that for a complex flow such as fuel spray, in which the dynamics are non-linear, POD modes embed multiple structures and therefore, multiple frequencies. Despite this, it is evident from Fig. 12 that modes 2 and 3 both display a dominant frequency at f=716 hz, while other minor amplitude peaks occur at 300 hz and 410 hz. The power spectral density (PSD) plots for the other test cases (see Tab. 2) are provided in the Appendix.

4.2 DMD Analysis

An improved understanding of the dynamical behaviour of the spray across the different test cases (Tab. 1) investigated can be gained from Fig. 13 (a-e), where the growth/decay rate is plotted against the corresponding frequency for all DMD modes. Large spatial and temporal scale structures are located close to the ordinate and are responsible for mixing and mass transfer at a macro-scale, while points associated to high frequency and high decay rate are linked to fine atomisation. As expected all σ are negative, which implies that all modes are subject to a sinusoidal oscillation whose amplitude decays at a faster rate as points are located further away from the abscissa. For example, when $\Delta p = 1$ bar several low frequency modes can be observed close to $\sigma = 0$, implying that associated structures will be highly coherent and exhibit an oscillation of nearly constant amplitude. As the pressure drop is increased, Δp=1, 2 and 15 bar (i.e. Fig. 13 a-c), data points gradually move further away from the abscissa, with virtually no points being present in $|\sigma|$ <20 s^{-1} for Δp=15 bar. This variation mainly affect the low frequency range, while the higher frequency decay rates are independent of the pressure drop. Essentially this implies that as the fuel pressure is increased (i.e. increasing Δp) structures are expected to become smaller in size and tend towards larger decay rates. This observation is corroborated when comparing data-sets for a fixed pressure drop (i.e. Fig. 13 c-e). The three plots are all characterised by the presence of very few modes for $|\sigma|$ <20 s^{-1}. However, this observation is less valid for 20F5A where some modes are in the range $|\sigma|$ <20 s^{-1}, but these are evenly spread across the frequency domain, while for the lower Δp conditions, 12F11A and 14F11A, data points are primarily located at low frequencies close to the ordinate. Based on these macro-considerations, it can be concluded that spray dynamics are mainly controlled by Δp, while only marginal variations to the $f - \sigma$ plane occurs when the ambient pressure is varied for a fixed pressure difference.

To identify the DMD modes related to the coherent structures partially discernible in Fig. 4 it is necessary to formulate some selection criteria and rank them in terms of significance. In the generation of Reduced Order Models associated to periodical

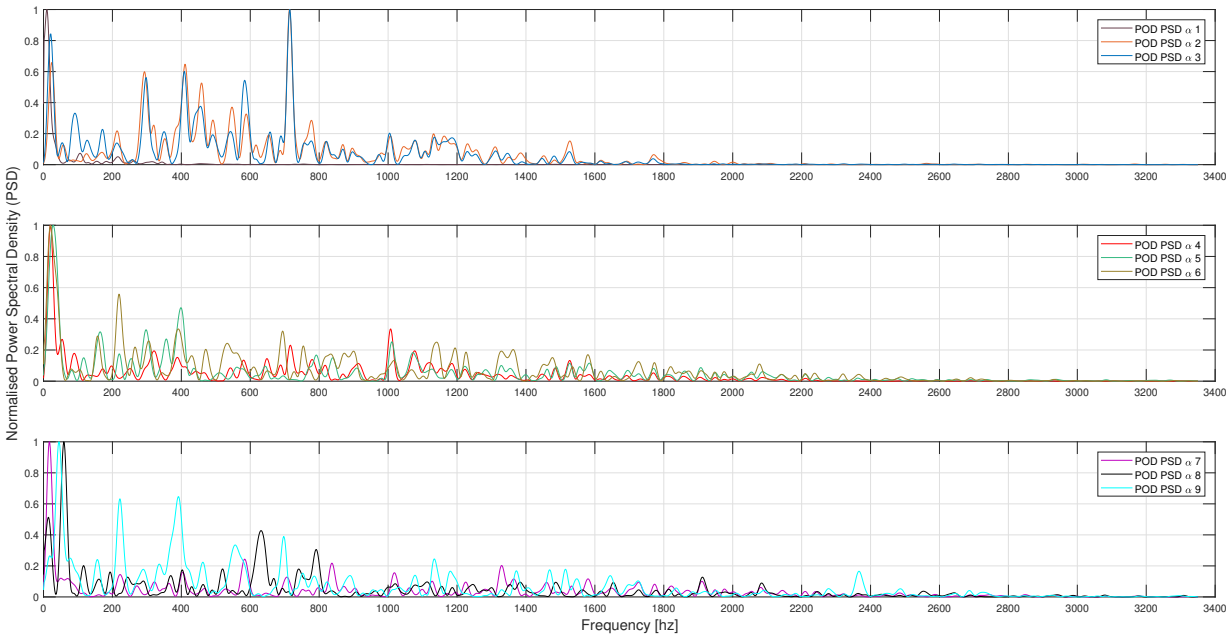

FIGURE 12. NORMALISED POWER SPECTRUM DENSITY (PSD) OF THE FIRST NINE POD MODES FOR THE REFERENCE TEST CASE, 26F11A (MEAN EXCLUDED).

flow fluctuations, like the spray instabilities investigated in this study, the decay rate is indicated as a preferable selection parameter [11], as the constant cyclic variation should be captured in modes lying on the abscissa of the $f-\sigma$ plane. However, most of the data points in Figs. 13 (a-e) are clustered in the range $-50 < \sigma < -20$ (see for example the base condition Fig. 13 c), resulting only in a marginal selection. A second selection parameter is represented by the initial amplitude of each mode, $\|\theta_{0i}\Phi_i\|$, with θ_{0i} corresponding to the magnitude of the temporal coefficient at $t = 0$. This approach is very limited because it increases the probability of selecting very high amplitude modes but heavily damped [15]. A third possibility corresponds to estimating the "energy" of each mode according to Eqn. (10)

$$E_i = \frac{1}{T}\int_0^T \|\theta_{0i}\ \Phi_i\ \mu_i^{t/\Delta t}\|^2 dt = \|\theta_{0i}\Phi_i\|^2\ \frac{e^{2\sigma_i T}-1}{2\sigma_i\ T} \qquad (10)$$

where T is the total time of the experiment.

This process is similar to that one used in POD, but it has to be stressed that in DMD the eigenvector base is not orthonormal and therefore the sum of the energy associated to each mode, E_i, does not match the total energy of the snapshots included in the data analysis. Nevertheless this coefficient combines the amplitude and the decay rate in a single coefficient, and can offer a viable parameter when comparing modes against those found in POD, which is energy based.

The variation of the energy, E_i, with frequency for the reference case 26F11A is shown in Fig. 14 (a). To reduce the scatter of the figure and facilitate the mode selection process the frequency domain was divided into equal segment of 50 hz, and the cumulative energy present in each segment is represented in Fig. 14 (a). In addition the cumulative "energy" accounts only for mode corresponding to low values of decay rate, i.e. $|\sigma\| < 100$ s^{-1}. Four peaks can be clearly distinguished at f =250, 750, 1500 and 2500 hz. A visual representation of the coherent structures associated to each dominant frequency is provided in Figs. 14 (b-e). These were obtained by superimposing the spatial modes present in each frequency segmentation. Several analogies in spray structures can be found between the DMD reconstructions of Figs. 14 (b) and (c) and the POD mode pairs 2-3 and 5-6 of Figs. 9 (b) and (e), respectively. In both cases the number of structures, axial displacement and level of staggering is consistent. Similarly, the DMD frequencies, 750 hz and 1500 hz could be related to the dominant frequency identified from the POD mode pairs 2-3 and 5-6 are $f = 716$ hz and $f = 1100$ hz, respectively (see Figs. 9 and 12). In POD the spatial structures are better resolved, but DMD clearly shows advantages in narrowing down the frequency of each structure within an accuracy of $\pm$ 25 hz. The structure associated to $f = 2500$ hz should appear in

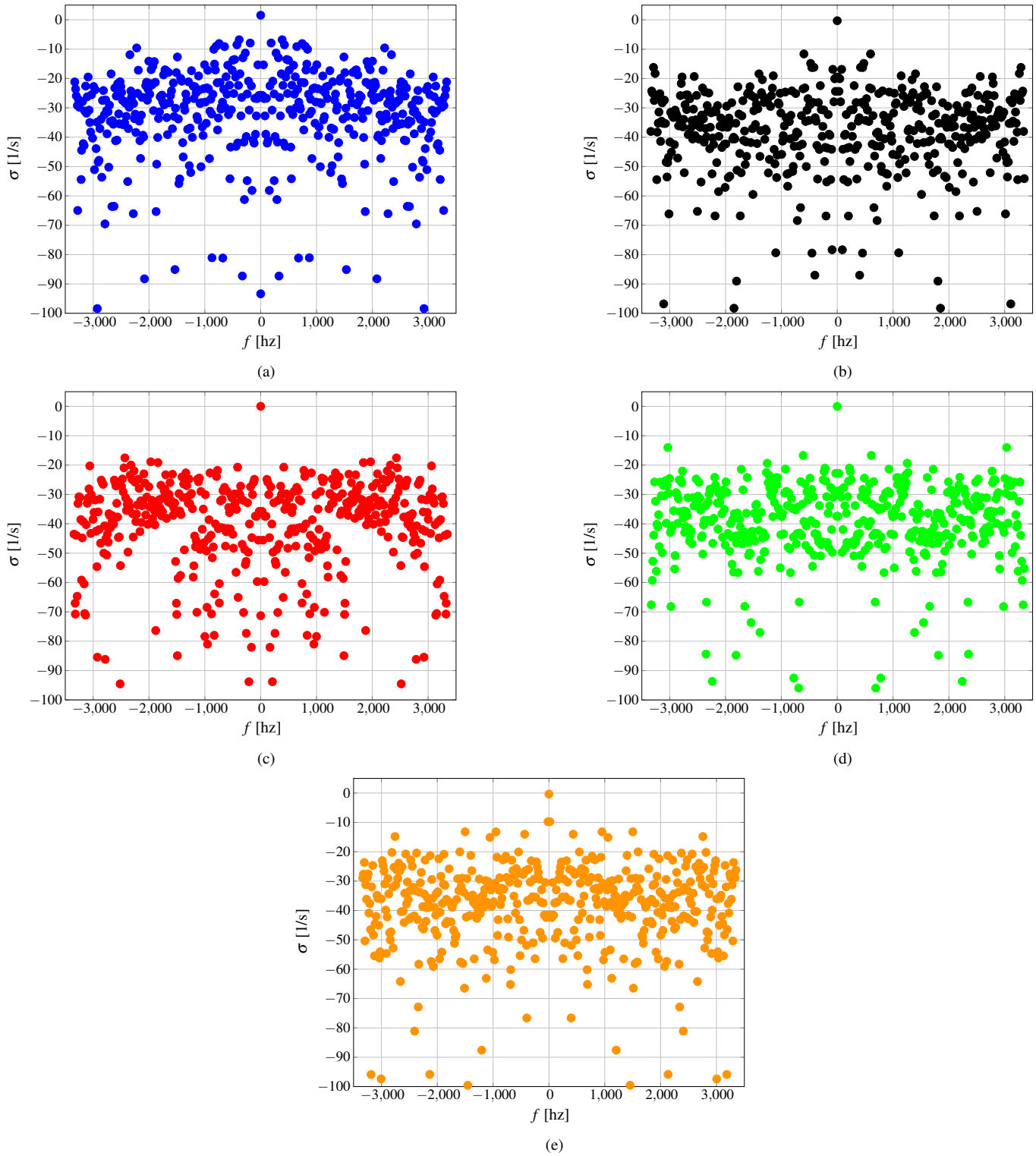

FIGURE 13. VARIATION OF THE DECAY RATE, σ, WITH FREQUENCY, f: (a) 12F11A, ●; (b) 14F11A, ●; (c) 26F11A, ●; (d) 16F1A, ●; (e) 20F5A, ●.

higher POD modes, which are not shown in Fig. 9.

A similar analysis was carried out for the other test cases, and corresponding dominant frequencies from POD and DMD analysis are presented in Tab. 2, and associated spatial modes are shown in Fig. 15. In addition, in Fig. 15 some higher DMD frequency modes have been shown, but these could not be identified in the first 9 POD modes.

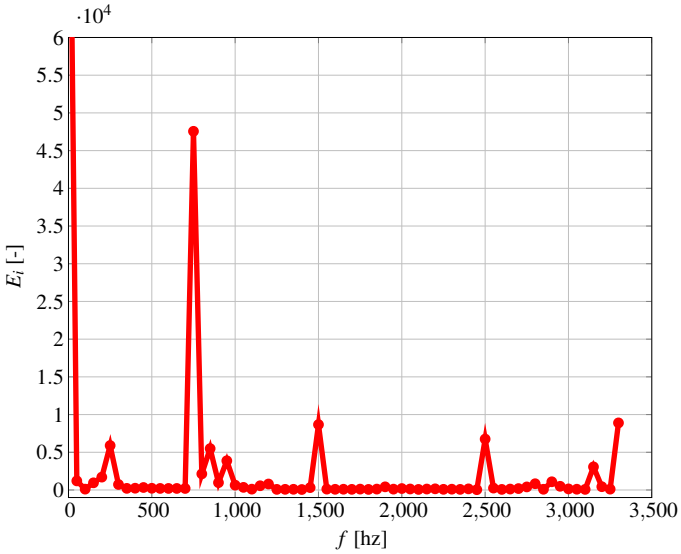

(a)

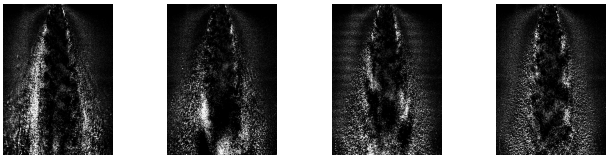

(b) f=250 hz (c) f=750 hz (d) f=1500 hz (e) f=2500 hz

FIGURE 14. (a) VARIATION OF THE CUMULATIVE ENERGY WITH INCREASING FREQUENCY; (b-e) RECONSTRUCTION OF THE SPRAY BASED ON MODES ASSOCIATED TO FREQUENCY RANGES CENTRED AT THE FOLLOWING FREQUENCIES; f =250, 750, 1500 and 2500 hz FOR 26F11A.

5 CONCLUSIONS

Dynamical characteristics of spray from a Siemens pressure swirl atomiser have been studied. A diesel surrogate, VISCOR calibration fluid, was sprayed into an optically accessible high pressure spray facility. The spray dynamics were captured with high speed laser planar imaging. In this study, two modal decomposition techniques - proper orthogonal decomposition (POD) and dynamic mode decomposition (DMD) - were applied. The effect of fuel injection and chamber pressures were studied using a range of test conditions that consist of (i) changing pressure difference, Δp, across the atomiser for a constant ambient pressure and (ii) changing ambient pressure for a fixed pressure difference Δp.

TABLE 2. CHARACTERISTIC FREQUENCIES IDENTIFIED FROM POD AND DMD ANALYSES FOR DIFFERENT TEST CASES.

Test case	f_{POD} [hz]	f_{DMD} [hz]
12F11A	120	200
14F11A	1100	1100
26F11A	300, 716, 1050	250, 750, 1500
16F1A	701, 1848, 2200	700, 1800, 2250
20F5A	359, 695, 1460	400, 700, 1450

Instantaneous images revealed presence of coherent structures, consistent with flow instabilities inherent to liquid fuel swirl atomisers. For all the cases, the POD mode shapes, ranked in the order of decreasing energy, indicated increased frequency (i.e. reduced inter-distance and size) of the observed coherent structures. The power spectra of these modes also reflected these observations. DMD analysis yielded frequencies which were consistent with observations from POD analysis.

With regard to the effect of change in Δp, POD analysis indicated that an increase in fuel injection pressure (at constant chamber pressure) increased the size of the coherent structures, which were observed to be further apart along the interface. DMD analysis showed that large scale coherent structures existed at lower fuel injection pressures, the decay rate of which decreased with increasing fuel injection pressures (i.e. increasing Δp).

POD analysis indicated that, similar to the effect of increase in Δp, the increase in the chamber ambient pressure (for constant Δp) also resulted in increased inter-distance between the coherent structures, which became increasingly oblong. This change in shape can be correlated to better spray quality (i.e. fine atomisation). No appreciable change in the decay rate of the modes was observed from DMD analysis, at constant Δp.

It is well known that atomisation can be improved by two approaches, either changing the pressure difference or the ambient pressure. However, the modal decomposition techniques employed in this work reveal that selection of the approach has a significant impact on the spatio-temporal characteristics of sprays.

ACKNOWLEDGMENT

The authors would like to acknowledge Siemens Industrial Turbomachinery Ltd. Lincoln, UK and EPSRC (EP/P003036/1)

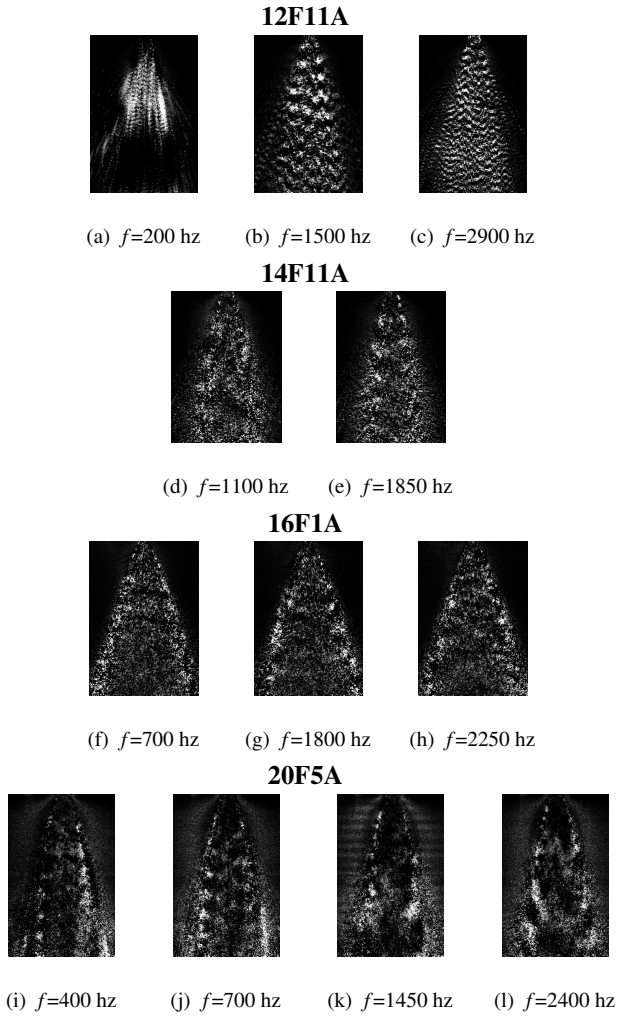

FIGURE 15. RECONSTRUCTION OF THE SPRAY BASED ON MODES ASSOCIATED TO DOMINANT FREQUENCIES FOR TEST CASES: 12F11A, 14F11A, 16F1A, 20F5A.

for their financial support, Dr Daniel Lörstad (Siemens, Sweden) for the insightful discussions and Dr Martin Hyde (TSI UK) for his support in laser imaging.

REFERENCES

[1] Reitz, R. D., and Bracco, F. V., 1982. "Mechanism of atomization of a liquid jet". *Physics of Fluids,* ***25***(10), pp. 1730–1742.

[2] Marmottant, P., and Villermaux, E., 2004. "On spray formation". *Journal of Fluid Mechanics,* ***498***, p. 73–111.

[3] Rajamanickam, K., and Basu, S., 2017. "Insights into the dynamics of spray–swirl interactions". *Journal of Fluid Mechanics,* ***810***, p. 82–126.

[4] Cheng, P., Li, Q., Kang, Z., and Chen, H., 2018. "Response of inner flow and spray characteristics of a pressure swirl injector to pressure oscillation in supply system". *Acta Astronautica*.

[5] Huang, C., Anderson, W. E., Harvazinski, M. E., and Sankaran, V., 2016. "Analysis of self-excited combustion instabilities using decomposition techniques". *AIAA Journal*, pp. 2791–2807.

[6] Ducci, A., Doulgerakis, Z., and Yianneskis, M., 2008. "Decomposition of flow structures in stirred reactors and implication for mixing enhancement". *Ind. Eng. Chem. Res.,* ***47***, pp. 3664–3676.

[7] Weheliye, W. H., Cagney, N., Rodriguez, G., Micheletti, M., and Ducci, A., 2018. "Mode decomposition and Lagrangian structures of the flow dynamics in orbitally shaken bioreactors". *Physics of Fluids,* ***30***(3), pp. 033603–1–13.

[8] Bourgouin, J. F., Moeck, J., Durox, D., Schuller, T., and Candel, S., 2013. "Sensitivity of swirling flows to small changes in the swirler geometry". *Comptes Rendus - Mecanique,* ***341***(1-2), pp. 211–219.

[9] Carlsson, H., Carlsson, C., Fuchs, L., and Bai, X. S., 2014. "Large eddy simulation and extended dynamic mode decomposition of flow-flame interaction in a lean premixed low swirl stabilized flame". *Flow, Turbulence and Combustion,* ***93***(3), pp. 505–519.

[10] Vinha, N., Meseguer-Garrido, F., De Vicente, J., and Valero, E., 2016. "A dynamic mode decomposition of the saturation process in the open cavity flow". *Aerospace Science and Technology,* ***52***, May, pp. 198–206.

[11] Tissot, G., Cordier, L., Benard, N., and Noack, B. R., 2013. "Dynamic Mode Decomposition of PIV Measurements for Cylinder Wake Flow in Turbulent Regime". In International Symposium on turbulence and shear flow phenomena (TSFP-8), pp. 1–6.

[12] Doulgerakis, Z., Yianneskis, M., and Ducci, A., 2011. "On the Manifestation and nature of macroinstabilities in stirred vessels". *AIChE Journal,* ***57***(11), pp. 2941–2954.

[13] de Lamotte, A., Delafosse, A., Calvo, S., and Toye, D., 2018. "Identifying dominant spatial and time characteristics of flow dynamics within free-surface baffled stirred-tanks from CFD simulations". *Chemical Engineering Science,* ***192***, dec, pp. 128–142.

[14] Cordier, L., Noack, B. R., Tissot, G., Lehnasch, G., Delville, J., Balajewicz, M., Daviller, G., and Niven, R. K., 2013. "Identification strategies for model-based control Topics in Flow Control.". *Experiments in Fluids,* ***54***(8), aug, p. 1580.

[15] Tissot, G., Cordier, L., Benard, N., and Noack, B. R., 2014. "Model reduction using Dynamic Mode Decomposition". *Comptes Rendus - Mecanique,* ***342***(6-7), pp. 410–416.

[16] Duwig, C., and Iudiciani, P., 2009. "Extended proper orthogonal decomposition for analysis of unsteady flames". *Flow, Turbulence and Combustion,* ***84***(1), Apr, p. 25.

[17] Gadiraju, S., Park, S., Gomez-Ramirez, D., Ekkad, S. V., Lowe, K. T., Moon, H.-K., Kim, Y., and Srinivasan, R., 2017. "Application of proper orthogonal decomposition to high speed imaging for the study of combustion oscillations". In ASME Turbo Expo 2017: Turbomachinery Technical Conference and Exposition, American Society of Mechanical Engineers, pp. V04BT04A031–V04BT04A031.

[18] Kypraiou, A., Allison, P., Giusti, A., and Mastorakos, E., 2018. "Response of flames with different degrees of premixedness to acoustic oscillations". *Combustion Science and Technology,* ***190***(8), pp. 1426–1441.

[19] Liu, K., Wood, J. P., Buchanan, E. R., Martin, P., and Sanderson, V. E., 2009. "Biodiesel as an Alternative Fuel in Siemens Dry Low Emissions Combustors: Atmospheric and High Pressure Rig Testing". *Journal of Engineering for Gas Turbines and Power,* ***132***(1), sep, pp. 11501–11509.

[20] Berkooz, G., Holmes, P., and Lumley, J. L., 1993. "The proper orthogonal decomposition in the analysis of turbulent flows.". *Ann. Rev. Fluid Mech.,* ***25***, pp. 539–575.

[21] Schmid, P. J., 2010. "Dynamic mode decomposition of numerical and experimental data". *J. Fluid Mech.,* ***656***, pp. 5–28.

[22] Brunton, S. L., Proctor, J. L., Tu, J. H., and Kutz, J. N., 2015. "Compressed sensing and dynamic mode decomposition". *J. Comput. Dyn.,* ***2***(2), pp. 165–191.

[23] Welch, P., 1967. "The use of fast fourier transform for the estimation of power spectra: a method based on time averaging over short, modified periodograms". *IEEE Transactions on audio and electroacoustics,* ***15***(2), pp. 70–73.

Appendix

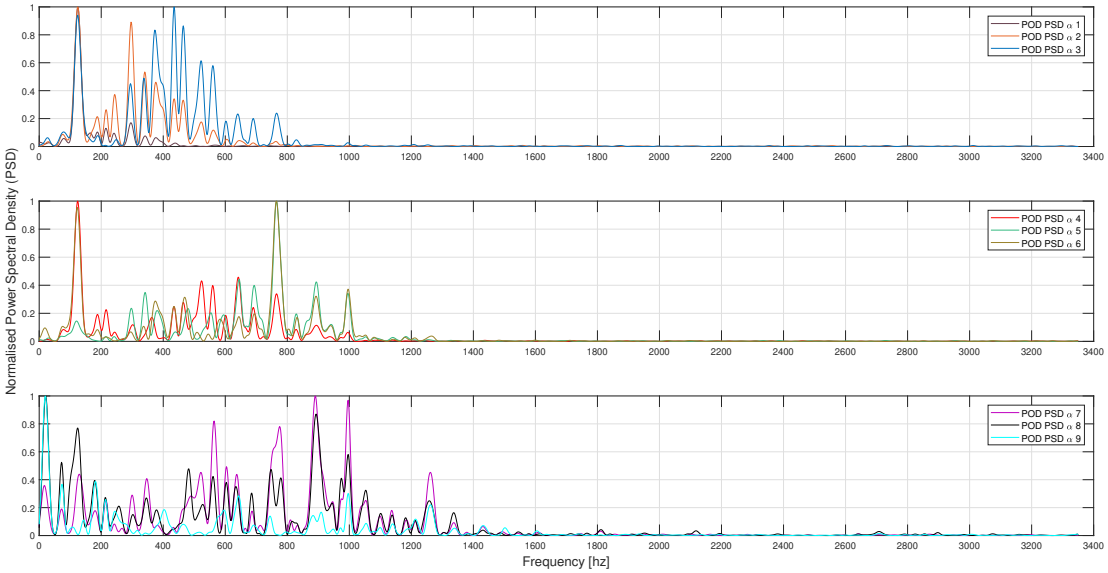

FIGURE A.1. NORMALISED POWER SPECTRUM DENSITY (PSD) OF THE FIRST NINE POD MODES FOR THE TEST CASE, 12F11A (MEAN EXCLUDED).

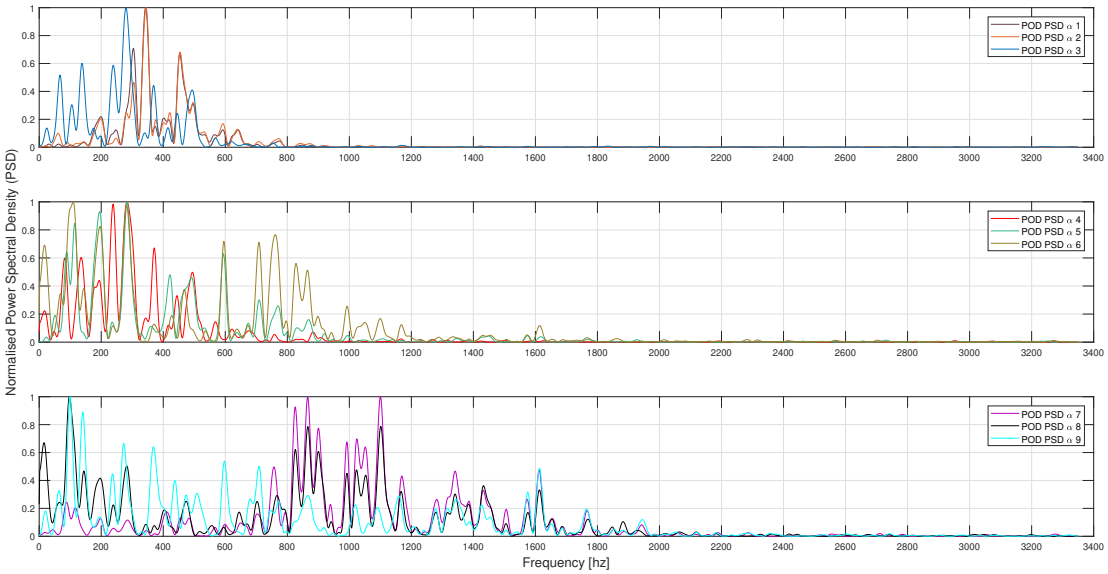

FIGURE A.2. NORMALISED POWER SPECTRUM DENSITY (PSD) OF THE FIRST NINE POD MODES FOR THE TEST CASE, 14F11A (MEAN EXCLUDED).

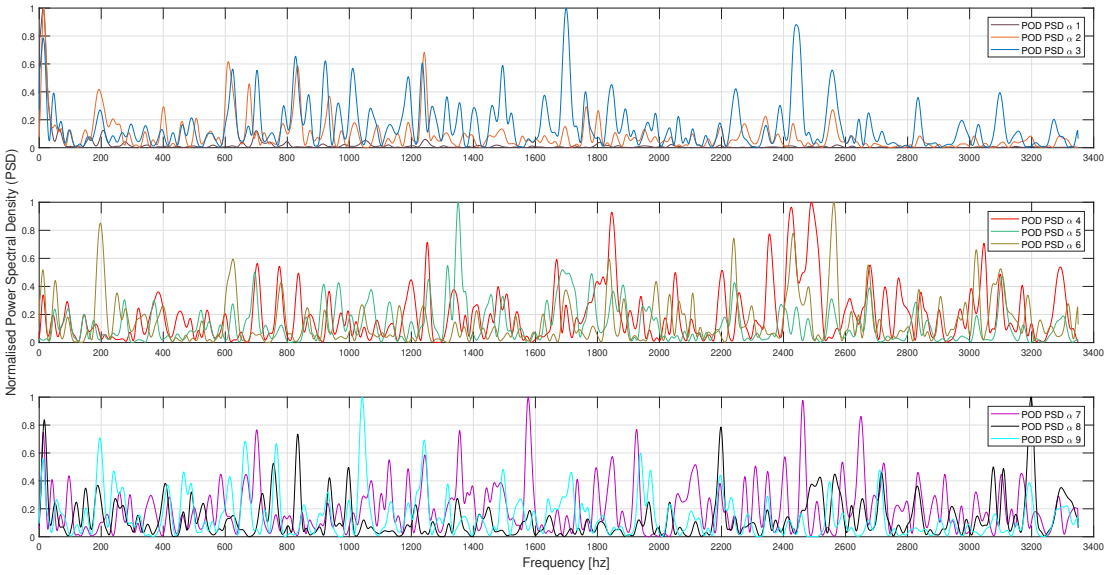

FIGURE A.3. NORMALISED POWER SPECTRUM DENSITY (PSD) OF THE FIRST NINE POD MODES FOR THE TEST CASE, 16F1A (MEAN EXCLUDED).

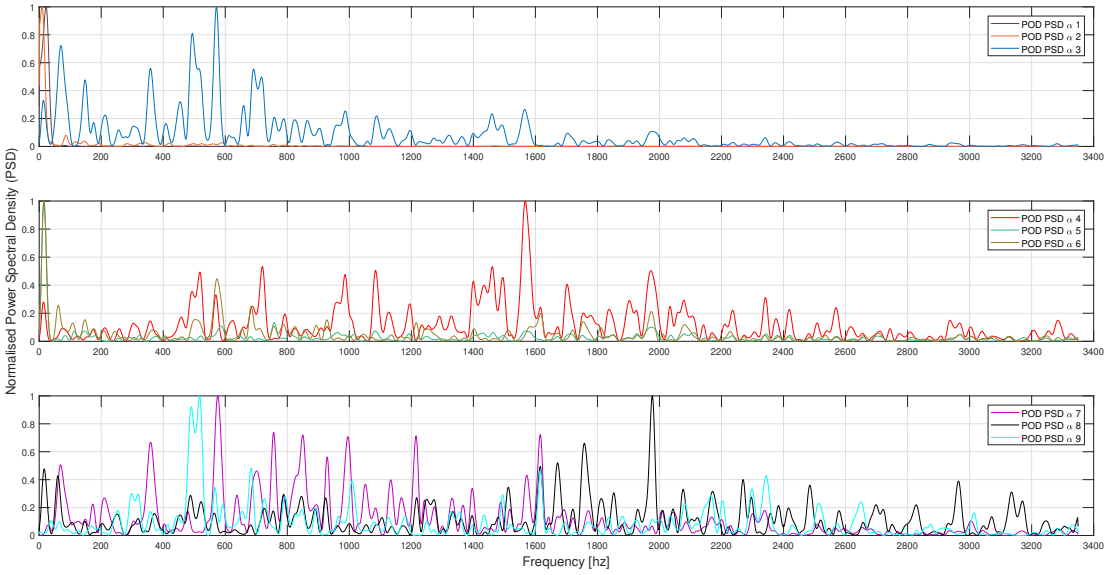

FIGURE A.4. NORMALISED POWER SPECTRUM DENSITY (PSD) OF THE FIRST NINE POD MODES FOR THE TEST CASE, 20F5A (MEAN EXCLUDED).